数理解析研究所講究録 1431 巻 2005 年 107-115

Stokes geometry for the quantized Hénon map in the horseshoe regime

Akira Shudo

Department of Physics, Tokyo Metropolitan University,
1-1 Minami-Ohsawa, Hachioji, Tokyo 192-0397, Japan
shudo@phys.metro-u.ac.jp

1, Quantum propagator of the Hénon map

A standard recipe to formulate quantum mechanics of the area-preserving mapping is first to construct the unitary operator generating the time evolution of quantum states. This is achieved by introducing discrete analog of the Feynman-type path integral:

$$< q_n|U^n|q_0 >= \int_{-\infty}^{\infty} \cdots \int_{-\infty}^{\infty} dq_1 dq_2 \cdots dq_{n-1} \exp\Big[\frac{i}{\hbar} S(q_0, q_1, \cdots, q_n)\Big]. \tag{1}$$

Here we take the coordinate representation. The function $S(q_0, \cdots, q_n)$ represents the discretized Lagrangian or the action functional given as

$$S(q_0, \cdots, q_n) = \sum_{j=1}^{n} \frac{1}{2}(q_j - q_{j-1})^2 - \sum_{j=1}^{n-1} V(q_j). \tag{2}$$

The action functional is derived so that applying the variational principle to generates the symplectic map. In fact, we can easily see that the condition $\partial S(q_0, \cdots, q_n)/\partial q_j = 0, \ (1 \leq j \leq n-1)$ yields the classical map in the Lagrangian form,

$$(q_{j+1} - q_j) - (q_j - q_{j-1}) = -V'(q_j). \tag{3}$$

If we take the potential function as

$$V(q) = -\frac{q^3}{3} - cq, \tag{4}$$

then the classical map is essentially the same as the so-called Hénon map, which is a non-trivial polynomial diffeomorphism generating chaos [1]. A canonical form of the Hénon map takes the form as

$$f : \begin{pmatrix} x \\ y \end{pmatrix} \mapsto \begin{pmatrix} y \\ y^2 - x + a \end{pmatrix}. \tag{5}$$

Here, the nonlinear parameter a is related with the parameter c in the potential function $V(q)$ as $c = 1 - a$.

A usual (complex) semicalssical scheme is just to take the leading order contribution in evaluating the multiple integral $< q_n|U^n|q_0 >$ by the stationary phase(or saddle point) method. The resulting semiclassical formula is expressed as a sum over contributions of classical trajectories connecting the initial and final states.

2. Anti-integrable limit and the horseshoe regime in the Hénon map

Introducing a new variable by $q_i' = \epsilon q_i$ and a new parameter $\epsilon = 1/\sqrt{-c}$, then the new action functional $\hat{S} = \epsilon^3 S$ is written as

$$\hat{S} = \epsilon\Big\{\sum_{j=0}^{n}\frac{1}{2}(q'_{j+1} - q'_j)^2\Big\} + \sum_{j=1}^{n}(\frac{q_j'^3}{3} + q'_j). \tag{6}$$

For $\epsilon \neq 0$ the variational condition $\partial S(q_0, \cdots, q_n)/\partial q_j = 0$ is equivalent to the explicit mapping rule (3). On the other hand, for $\epsilon = 0$ there no more exist such explicit relations between successive points. The "orbits" for $\epsilon = 0$, which are expressed as $q_i \in \{-1, +1\}$ $(i \in \mathbb{Z})$. This limit is called anti-integrable limit [2].

The next simplest situation is the parameter region where the so-called horseshoe condition is satisfied. To be precise, we give the definition of the horseshoe condition: Let $\Omega(f|_{\mathbb{R}})$ be the non-wondering set of the real Hénon map $f|_{\mathbb{R}}$, and let

$$\Lambda = \bigcap_{k=-\infty}^{\infty} f^k(S)|_{\mathbb{R}},$$

where the square $S = \{(x, y) \mid |x| \leq R, |y| \leq R\}$ is given for a sufficiently large R. The Hénon map f is said to satisfy the horseshoe condition if there exists a continuous semi-conjugacy of $\Omega(f|_{\mathbb{R}})$ onto the 2-shift, that is, every trajectory has its own infinite binary symbol sequence in forward and backward directions.

It was proved that the Hénon map is hyperbolic and conjugate to the 2-shift up to when the first tangency occurs [3]. Here, we mean the first tangency by the first homoclinic tangency between the uppermost stable manifold and innermost unstable manifold of a saddle fixed point on the real plane(see Fig. 1). A numerical study shows that the first tangency parameter value is evaluated as $a_c = 5.699311\cdots$ [4]. For $a > a_c$, the invariant set Λ coincides with the Julia set J and is confined on the real plane. we here focus our attention to such a case.

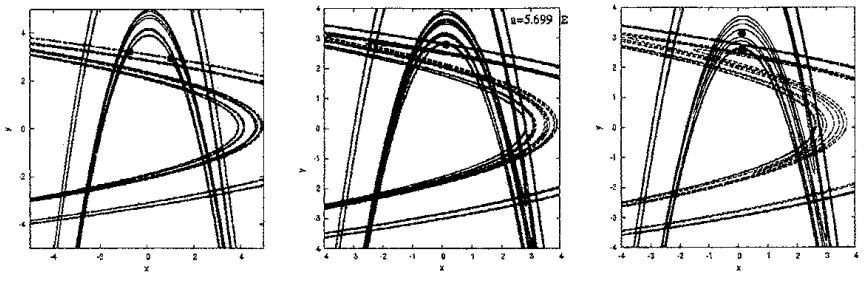

Figure 1: Stable and unstable manifolds before and after the first tangency.

3. Stokes geometry in the horseshoe regime

In what follows, we shall fix the initial coordinate $q_0 = \alpha$ and regard the quantum propagator (1) as a function of the final coordinate q_n. We therefore use the notation

$I(q_n) \equiv < q_n|U^n|q_0 >$ to represent the multiple integral defined in eq. (1). As will be seen below, we put aside q_0 dependence for the moment.

Since we have differential equations acting on our multiple integral (1) [5], we can apply a prescription to construct the Stokes geometry for higher-order differential equations to our integral $I(q_n)$ [7]. Concerning turning points, we say the point q_n^T is a turning point, if the q_n^T satisfies the following conditions:

$$\frac{dq_n^T(q_0, q_1)}{dq_1} = 0,$$
$$\frac{dS(q_0, \cdots, q_n^T(q_0, q_1))}{dq_1} = 0.$$

Also we follow the definition of virtual turning points, that is, for $q_1^{(i)} \neq q_1^{(j)}$, q_n^T is a virutal turning point if

$$q_n^T(q_0, q_1^{(i)}) = q_n^T(q_0, q_1^{(j)})$$
$$S(q_0, q_1^{(i)}, \cdots, q_n^T(q_0, q_1^{(i)})), = S(q_0, q_1^{(j)} \cdots, q_n^T(q_0, q_1^{(j)})).$$

In the same way, we can apply the definition of Stokes curves. Recalling the generating relation, $\partial S(q_0, \cdots, q_n)/\partial q_n = q_1$, we say the curves emanating from the turning points q_n^T and satisfying the following relation;

$$\mathrm{Im}\, S(q_0, q_1^{(i)}, \cdots, q_{n-1}^{(i)}, q_n^T) = \mathrm{Im}\, S(q_0, q_1^{(j)}, \cdots, q_{n-1}^{(j)}, q_n^T). \tag{7}$$

Stokes curves emanating from ordinary turning points give the ordinary Stokes curves, and those from virtual turning points give new Stokes curves.

A typical example of the Stokes geometry in the horseshoe regime at $n = 3$ is shown in Fig. 2. The most important fact is that all the turning points in the ordinary sense are located on the real axis. As also presented in Fig. 3, this reflects the fact that all the folding points of Lagrangian manifolds appear on the real plane, which is characteristic of the horseshoe property of the Hénon mapping. There are three virtual turning points, one of which are sited on the real axis and the others in the imaginary domain. It should be noted that, due to the symmetry of the Stokes graph with respect to the real axis, a degenerated crossing point on the real axis appears on the real axis. Four ordinary Stokes curves and two new Stokes curves cross there and the univaluedness condition around it determines characters of each Stokes curve uniquely [5].

The most urgent issue in our interest to clarify the relation between classical dynamics generating chaos and the corresponding Stokes geometry. In the classical side, stretching and folding is a key mechanism generating chaos, and the number of folding points of the Lagrangian manifold increases exponentially as a function of the time step n. The folding points of the Lagrangian manifold manifest themselves as the turning points in Stokes geometry. Figure 3 depicts *time evolution of Stokes graphs* together with the corresponding Lagrangian manifolds. Here, only the ordinary Stokes curves are drawn. Three Stokes curves emanate from a simple turning point, and local Stokes

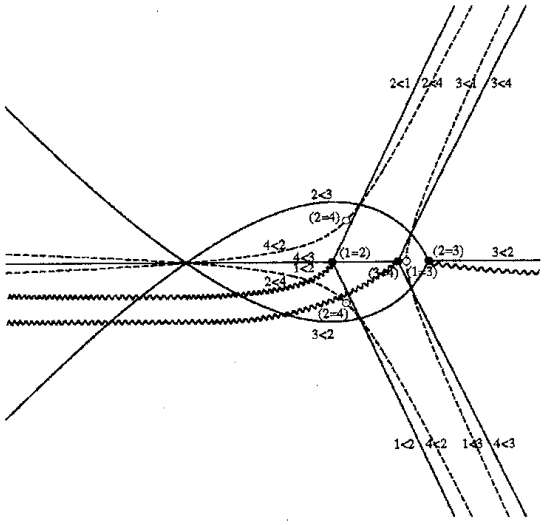

Figure 2: Stokes geometry for the Hénon map for $n = 3$. The dominance relation and types of the turning points follow the usual convention. Filled dots and open dots represent ordinary and virtual turning points, respectively. Broken lines new Stokes curves.

geometry in the vicinity of folding points can be well understood within conventional arguments.

As seen from Fig. 3, some ordinary Stokes curves rotate around the origin several times, the number of rotation increases with the time step n. It would be difficult to find out the rule controlling the behavior of Stokes curves as a function of n only by observing them on q_n plane. However, plotting the Stokes curves on the q_1 plane, one can more easily understand the structure of Stokes curves. Here we note that q_1 plays the role of time in the bicharacteristic equations for the differential operator acting on the $I(q_n)$ [5].

In Fig. 4, the ordinary Stokes curves are drawn on q_1 plane, The structure of Stokes curves are much simpler that those on q_n plane. Using this representation, one can derive the how the Stokes curves behave on q_n. We here provide only the result (see details in [5]):

$$\sharp\{\text{Ordinary turning points}\} :$$
$$T^{(n)} = 2^n - 1$$
$$\sharp\{\text{Ordinary Stokes curves in group } j\} :$$
$$S_j^{(n)} = 2^{n-j}$$
$$\sharp\{\text{Rotation around the origin in group } j\} :$$
$$R_j^{(n)} = \left\{2^{n-j} - 1 - \left[\frac{2^{n-j}-1}{3}\right]\right\}/2$$

Here $[\cdot]$ denotes the Gauss symbol.

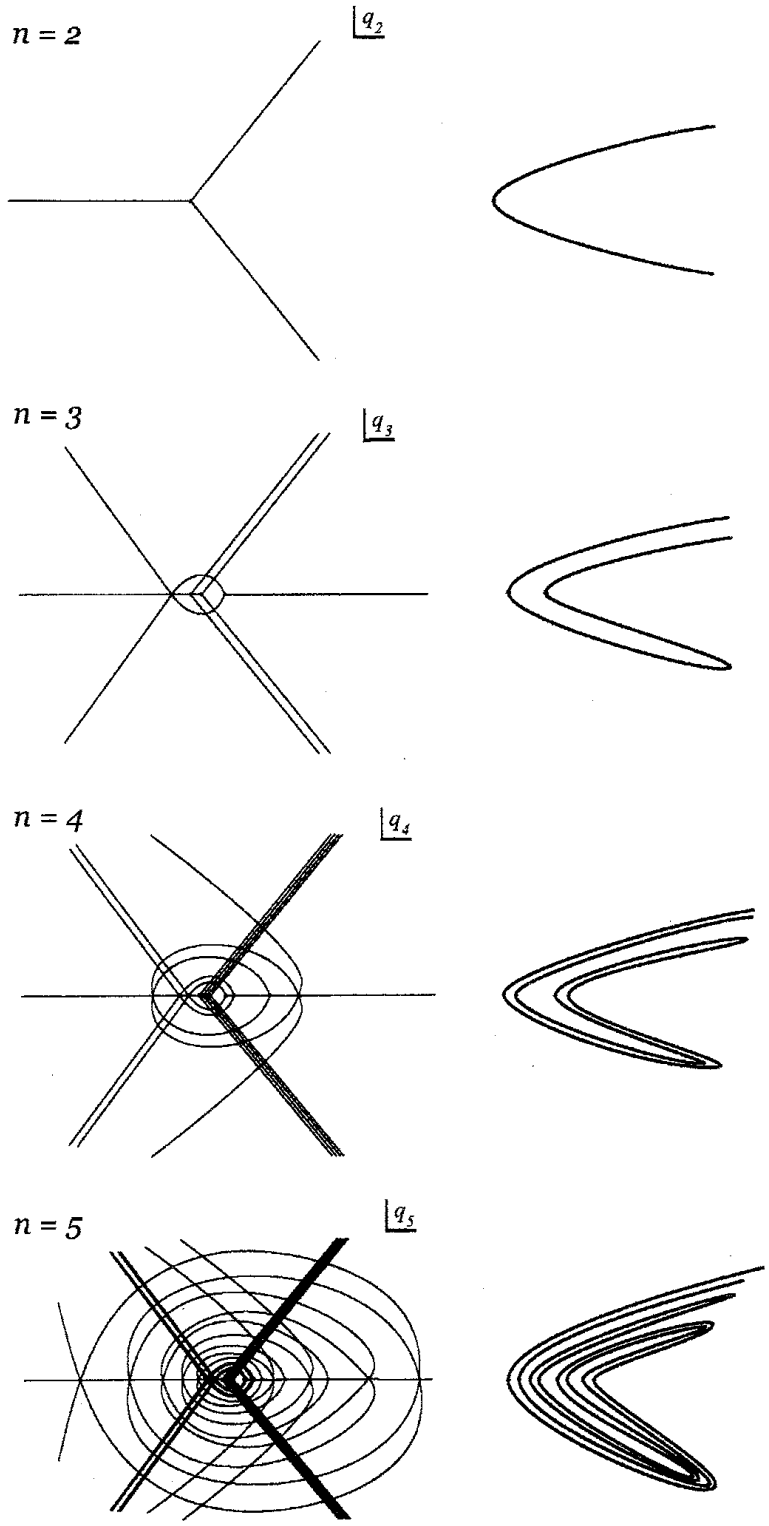

Figure 3: Time evolution of Stokes geometry for the Hénon map. The left row represent the ordinary Stokes curves and right row Lagrangian manifolds starting from the initial state $q_0 = 0$. These are drawn on the (q_{n-1}, q_n) plane.

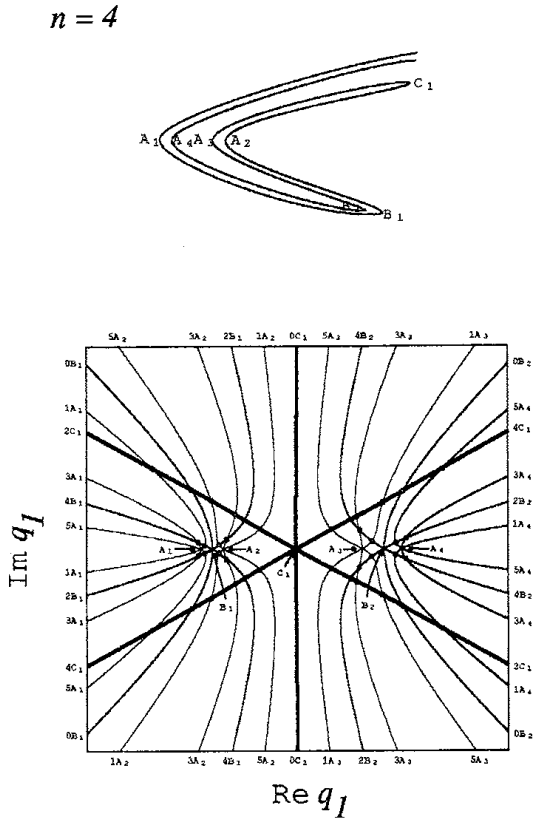

Figure 4: The Lagrangian manifold at $n = 4$(upper figure), and the Stokes curves on q_1 plane(lower figure). The bold, normal and thin lines represent the Stokes curves which appear at $n = 2$, $n = 3$ and $n = 4$, respectively. The turning points labeled as C_i, B_i and A_i on the Lagrangian manifold are aligned on the real line on q_1 plane.

Concerning the virtual turning points and new Stokes curves, we only have a conjecture based on numerical observations. As shown in Fig. 6, virtual turning points appearing in the Stokes geometry in the horseshoe parameter region are classified into two types: the first ones are those located on the real axis, and the second ones on the purely complex domain. Numerical observations tell us that the second-type virtual turning points cross the real axis only once and crossing points are either the degenerated one shown in Fig. 2 or the normal one at which three Stokes curves cross each other [5].

Therefore, in order to have the connection matrix $\mathbb{T}$, which is the most relevant physical quantity in our interest [8, 9], it is suffice to examine how the connection occurs along real axis. Here the connection matrix $\mathbb{T}$ relates the WKB solutions at Re

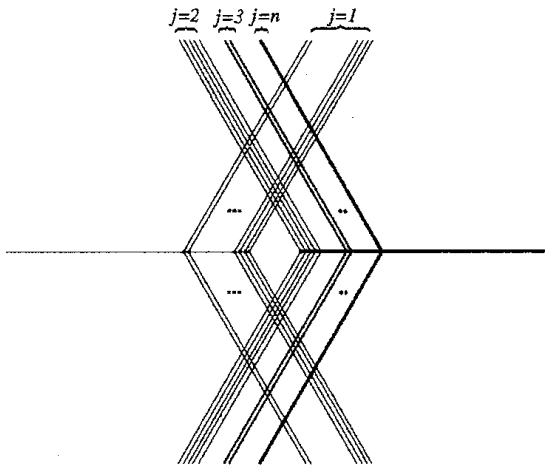

Figure 5: The ordinary Stokes curves on q_n plane. This is a schematic picture and only the Stokes curves around the origin are drawn . The index j represent at which time step the Stokes curves appear. For example, the Stokes curves for $j = n$ appear in at the first step, and those for $j = 2$ appear in the final step n.

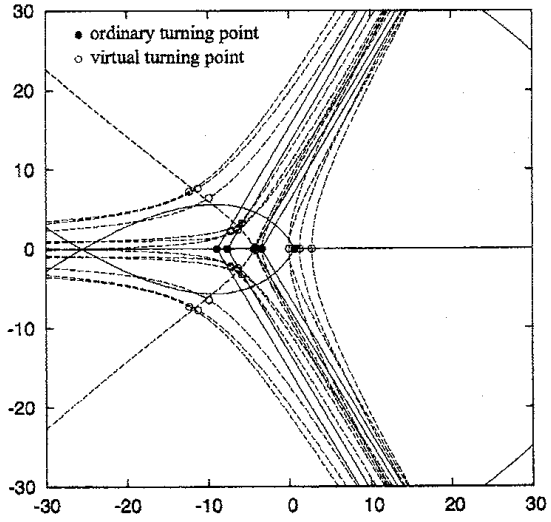

Figure 6: The ordinary(solid lines) and new(broken lines) Stokes curves for $n = 4$. Here, characters of Stokes curves are not indicated. Other turning points and Stokes curves are outside the figure, but the location of virtual turning points is classified into two types described in the text.

$q_n = -\infty$ and those at Re $q_n = \infty$ as

$$\begin{pmatrix} \varphi_1^{(\infty)}(q_n) \\ \varphi_2^{(\infty)}(q_n) \\ \vdots \\ \varphi_{2^n}^{(\infty)}(q_n) \end{pmatrix} = \mathbb{T} \begin{pmatrix} \varphi_1^{(-\infty)}(q_n) \\ \varphi_2^{(-\infty)}(q_n) \\ \vdots \\ \varphi_{2^n}^{(-\infty)}(q_n) \end{pmatrix}.$$

In this respect, the first-type virtual turning points and new Stokes curves emanating from them do not play any role since the Stokes coefficients in the vicinity of virtual turning points should be zero. Therefore, the problem is reduced to finding in which order degenerated and normal crossing points appear along the real axis. The second-type virtual turning points are involved in such crossing points. We have obtained an algorithm, using a graphical representation of crossing points aligned along the real axis, to derive the connection matrix $\mathbb{T}$ in the horseshoe regime (see details also in [5]).

4. Concluding remarks

In this report, we have sketched the Stokes geometry of quantized Hénon map in the horseshoe regime. A primary motivation of our work originates from recent success of complex semiclassical description of quantum tunneling especially in the presence of chaos [8, 9, 10]. In such a program, the understanding of Stokes phenomena is a critical step to make our analysis self-containd. Our prescriptions to treat the Stokes phenomenon occurring in our quantum propagator are based on the exact WKB analysis, which naturally introduces novel ingredients in Stokes phenomena in higher-order differential equations [6, 7].

The strategy we took first was to select out the simplest possible chaotic system suitable for our purpose. The Hénon map would be the best candidate that meets such a requirement and the horseshoe regime is the simplest possible situation. Thus, analyzing Stokes geomety in the horseshoe limit would be the first target to be investigated. If the situation for the horseshoe limit is well understood, one way to step forward is to trace Stokes geometry as a function of the system parameter a, and focus on bifurcation phenomena [11, 5]. As stressed already, in the horseshoe case, all the turning points are located on the real plane, but as the nonlinear paremeter a decreases, some of them fall into purely imaginary plane. Such an event occurs as a result of coalescence of turning points. If we know how the Stokes graph changes when such a bifurcation phenomenon occurs, the Stokes geometry in a generic parameter value can be traced from the anti-integrable limit in principle. This is exactly the same strategy to study the *pruning* of the horseshoe structure [12].

0.1 Acknowledgments

The author is grateful to T. Aoki, T. Kawai, and Y. Takei for their valuable comments and discussions. This work is based on the collaboration with K.S. Ikeda, which is announced as ref. [5].

References

[1] S. Friedland and J. Milnor, Ergod. Theor. Dyn. Sys. **9**(1989)67.

[2] S. J. Aubry and G. Abramovici, Physica D, **43** (1990) 199; S.J. Aubry, Physica D **86** (1995) 284.

[3] E. Bedford and J. Smillie, math. DS/0103038.

[4] D. Sterling, H.R. Dullin and J.D. Meiss, Physica D **241** (1999) 153.

[5] A. Shudo and K.S. Ikeda, to be submitted.

[6] H.L. Berk, W.M. Nevins and K.V. Roberts, J. Math. Phys., **23**(1982) 988.

[7] T. Aoki, T. Kawai and Y. Takei, in Analyse algébrique des perturbations singulières. I. (ed. by L. Boutet de Monvel) Hermann, (1994) 69.

[8] A. Shudo and K. S. Ikeda, Phys. Rev. Lett. **74**, 682 (1995); Physica D**115**, 234 (1998); T. Onishi, A. Shudo, K.S. Ikeda, and K. Takahashi, Phys. Rev. E **64**, 025201(R) (2001).

[9] A. Shudo, Y. Ishii and K.S. Ikeda, J. Phys. A. **35** (2003) L225; A. Shudo, Y. Ishii and K.S. Ikeda, to be submitted.

[10] K. Takahashi and K. S. Ikeda, Ann. Phys. (NY) J. Phys. A. **283** 94; J. Phys. A **36** (2003) 7953.

[11] T. Aoki, T. Kawai, S. Sasaki, A. Shudo and Y. Takei, *Virtual turning points and bifurcation of Stokes curves for higher order ordinary differential equations*, J. Phys. A, in press.

[12] P. Cvitanović, G. Gunaratne and I. Procaccia, Phys. Rev. A **38** (1988) 1503.